IEEE Access
Multidisciplinary | Rapid Review | Open Access Journal

Received 8 June 2023, accepted 22 June 2023, date of publication 28 June 2023, date of current version 6 July 2023.

Digital Object Identifier 10.1109/ACCESS.2023.3290322

RESEARCH ARTICLE

OTFS Based SAR With Low Complexity Receiver

GAURAV SHARMA, (Graduate Student Member, IEEE), AND A. AROCKIA BAZIL RAJ, (Senior Member, IEEE)
Department of Electronics Engineering, Defence Institute of Advanced Technology, Pune 411025, India
Corresponding author: Gaurav Sharma (gauravsharma70@gmail.com)

ABSTRACT Synthetic aperture radar (SAR) are exploiting millimeter-wave (mmWave) band for imaging applications. However, with the conventional pulse-width of few tens of microseconds the receive SAR signal experiences intra-pulse Doppler shift in mmWave band which results in severe image degradation. The recently proposed, orthogonal time frequency space (OTFS) modulation has shown to be resilient against the Doppler impairments. In this work, we propose a cyclic-prefix (CP)-OTFS modulation with practical pulse shaping waveforms for SAR applications. We present a novel delay-Doppler domain based pulse compression technique to mitigate the intra-pulse Doppler impairments. The traditional pulse compression techniques in SAR are known to have inter-range-cell-interference (IRCI) due to the presence of range side-lobes which leads to low resolution imaging. The proposed receiver algorithm effectively exploits the diagonalization property of factor-circulant matrix and eliminates IRCI. The receiver algorithm is shown to have a lower computational complexity vis-a-vis the state-of-the-art matched-filter OTFS radar receiver thus, making it suitable for real-time SAR applications. Finally, simulated SAR images show the effectiveness of our methodology in eliminating the distortion caused by intra-pulse Doppler shift and removal of IRCI for high resolution imaging.

INDEX TERMS Inter range cell interference (IRCI), intra-pulse Doppler, orthogonal time frequency space (OTFS), synthetic aperture radar (SAR).

I. INTRODUCTION

Synthetic aperture radar (SAR) is an imaging device with a wide range application in both civil and military domain. SAR is known to have imaging capabilities of natural and man-made objects in all day and weather conditions [1], [2], [3]. Traditionally, SAR are operated in X-band or lower frequency bands however, these bands are extensively occupied and requirement of large bandwidths for high resolution imaging cannot be fulfilled. As an alternative, high frequency millimeter-wave (mmWave) band which offers large swath of bandwidths is being explored by the radar research community for SAR imaging applications [4], [5], [6]. The extensive advancements in the field of mmWave massive multiple-input-multiple-output (MIMO) antenna technology [7], [8] is proving to be a key enabler for mmWave band radar operations and it is now also leveraged for radar applications [9], [10], [11].

The mmWave offers high resolution SAR imaging however, with a pulse-width of few tens of microseconds the receive SAR signal experiences a discernible intra-pulse Doppler shift due to millimeter wavelengths. It is known that the transmit pulse should be long enough for the radar to emit sufficient energy so that the received echo is detectable by the receiver [12]. Hence, without compromising with the transmit energy of the signal the intra-pulse Doppler shift needs to be compensated, which otherwise will impair the received signal and adversely impact SAR imaging capabilities. Therefore, an appropriate signal processing technique needs to be formulated to counter the effects of intra-pulse Doppler experienced by SAR in mmWave band.

The SAR transmit pulse has a long duration due to which, the reflected signal from the scatterers is overlapped with each other on reception at the receiver. These superimposed echoes have a natural interference wherein, the reflected

The associate editor coordinating the review of this manuscript and approving it for publication was Fabrizio Santi.

energy from one scatterer interferes with the other. To overcome this interference the conventional SAR utilizes an LFM (Linear Frequency modulation)-based transmit pulse [1], [2], [3] which has a large bandwidth as well as a large pulse duration. The receiver exploits the pulse compression technique, which yields narrow compressed pulses thus, making the receive signal distinguishable for different range cells. However, the pulse compression also results in interference of energy from the adjacent range cells due to the side-lobes of the ambiguity function of an LFM pulse. The magnitude of the side-lobe is approximately $\sqrt{L}$, if the magnitude of the main lobe is L. These undesirable side-lobes in range profiling of a SAR system are termed Inter-range-cell interference (IRCI). Thus, such receivers with range side-lobes are unsuitable for high resolution imaging. Orthogonal frequency division multiplexing (OFDM) and Frequency domain system identification (FDSI) were proposed to mitigate IRCI for both single-input-single-output (SISO) [13], [14] and MIMO [15], [16] SAR, respectively for high resolution IRCI-free imaging however, these systems fail to counter the effects of intra-pulse Doppler shift. Thus, exploration of newer waveforms and signal processing techniques is required to collectively mitigate the effects of intra-pulse Doppler shift and IRCI.

Orthogonal time frequency space (OTFS) modulation was recently proposed with delay-Doppler domain based signal processing [17]. This new modulation scheme was shown to be robust against Doppler shift impairments in time-varying channels. OTFS-based radar system has been proposed for conventional range and velocity estimation [18] applications. OTFS is shown to counter Doppler however, the proposed use of matched-filter fails to remove IRCI. Thus, if SAR applications desire to take advantage of OTFS, a new methodology to eliminate IRCI is required for high resolution imaging.

Low complexity receiver algorithms for OTFS modulation based wireless communication systems are a key research area for its efficient implementation. In [19] and [20] the authors have proposed low complexity minimum mean square error (MMSE) OTFS receiver based on OTFS channel sparsity. The authors in [21] have proposed an efficient transform-domain maximal ratio combining detection method which exploits the Doppler diversity and is free of any matrix inversion. On the similar lines, receivers with low computational complexity for OTFS-based SAR are also desirable for real-time applications. In [22], the authors have proposed a real-time SAR imaging methodology for large-scale scenes using an observation-based sparse imaging with some approximations. In [6], a MIMO-SAR imaging technique is proposed for enhancing azimuth resolution for autonomous driver assistance in vehicles. Hence, with the envisaged real-time applications for SAR, a low complexity receiver is more practicable from the implementation point of view.

OTFS modulation scheme is yet to be explored for the multifarious requirements of SAR which motivated the authors to investigate OTFS modulation for SAR imaging. In this paper, we propose cyclic-prefix (CP)-OTFS-based SAR and, the key contributions are summarized as under.

- We derive a novel pulse compression algorithm for CP-OTFS-based SAR. The proposed algorithm is shown to be capable of removing IRCI from the range profiling and offering high resolution imaging. The technique achieves IRCI-free high resolution imaging with a pulse compression gain similar to that of a conventional LFM-based radar system.
- We exploit the Doppler resilience of OTFS modulation by incorporating delay-Doppler domain based signal processing. This methodology effectively mitigates the distortion caused by intra-pulse Doppler shift in SAR imagery. The mitigation is achieved concurrently with IRCI-free pulse compression.
- Through the use of the diagonalization property of factor-circulant matrix, we reduce the computational complexity of the receiver to $O(MNlog_2(MN))$ vis-a-vis $O(M^2N^2)$ of the matched-filter OTFS radar [18], where N and M represent number of symbols and number of subcarriers, respectively.

The paper is organized in the following manner. In Section II, we introduce the system model of CP-OTFS-based SAR and present a corresponding delay-Doppler channel model. Section III proposes our low-complexity receiver design for CP-OTFS-based SAR. We also present the signal-to-noise ratio (SNR) analysis after the proposed range compression technique. In Section IV, the computational complexity of proposed pulse compression algorithm is presented along with some simulation results. Finally, in Section V we conclude the paper with our remarks.

Notations: The notations followed in this paper are: $\mathbf{X}$, $\mathbf{x}$, x represent matrix, vector and scalar, respectively. $\mathbb{C}^{M\times N}$ represents $M \times N$ matrix with complex entries, $\mathbf{I_M}$ denote the M-dimensional identity matrix and $diag(\mathbf{x})$, the diagonal matrix with elements of $\mathbf{x}$. $\mathbf{F_n} = \{\frac{1}{\sqrt{n}} e^{-j2\pi kl/n}\}_{k,l=0}^{n-1}$ and $\mathbf{F}_\mathrm{n}^\mathrm{H}$ denote the n-point DFT and the IDFT matrices, respectively. The scalar $W_N = e^{-j\frac{2\pi}{N}}$, $\lceil\cdot\rceil$ denotes the ceil operator, $\mathbf{vec}(\mathbf{X})$, the column-wise vectorization of the matrix $\mathbf{X}$, $[\cdot]_n$, the mod-n operation, $\circ$, the Hadamard product and $\oslash$, the Hadamard division.

II. SYSTEM MODEL FOR CP-OTFS SAR

In this section, we present the system model for CP-OTFS-based SAR and corresponding delay-Doppler channel model for a SAR scenario.

A. CP-OTFS SAR MODULATOR

The OTFS modulator places MN input complex weights $x_{l,k}$ (M and N are some positive integers) in a delay-Doppler grid as $M \times N$ matrix $\mathbf{X} = \{x_{l,k}\}, l \in [0, M-1], k \in [0, N-1]$. The delay-Doppler domain matrix $\mathbf{X}$ is converted to the time-frequency domain by applying Inverse Symplectic

Fast Fourier Transform (ISFFT) as

$$\mathbf{X}_{\text{tf}} = \mathbf{F}_{\text{M}}\mathbf{X}\mathbf{F}_{\text{N}}^{\text{H}} \tag{1}$$

The time-frequency domain signal has N symbols of duration T and M sub-carriers with spacing $\Delta f = 1/T$. Then "Heisenberg transform" is applied to $\mathbf{X}_{\text{tf}}$ to obtain a delay-time domain signal. The transform is implemented by an M-point Inverse Fast Fourier Transform (IFFT) followed by pulse-shaping with a pulse g_{tx} of duration $(0, T]$. The $M \times N$ delay-time matrix is expressed as

$$\mathbf{S} = \mathbf{G}_{\text{tx}}\mathbf{F}_{\text{M}}^{\text{H}}\mathbf{X}_{\text{tf}} \tag{2}$$

where $\mathbf{G}_{\text{tx}}$ is the diagonal matrix with entries as samples of g_{tx}: $\mathbf{G}_{\text{tx}} = \mathbf{diag}\left(g_{tx_0}, g_{tx_1}, \ldots, g_{tx_{(M-1)}}\right)$. We choose, g_{tx} to be a rectangular pulse which reduces $\mathbf{G}_{\text{tx}}$ to $\mathbf{I}_{\mathbf{M}}$. Finally, the time domain OTFS samples are generated by column-wise vectorization of $\mathbf{S}$

$$\mathbf{s} = \mathbf{vec}\,(\mathbf{S}) \tag{3}$$

The time domain signal has a duration of NT (without CP) and bandwidth of $M\Delta f$ with $K = MN$ samples at an interval $T_s = 1/M\Delta f$. We append a CP of length $(L-1)$ to the time domain OTFS samples, where L corresponds to number of range cells in swath. The value of L is evaluated as $L = \left\lceil (\tau_{max} - \tau_{min})/T_s \right\rceil$, where τ_{max} and τ_{min} are the maximum and minimum delays of received echo from swath, respectively. The CP length in SAR application is equivalent to the maximum delay estimation in matched-filter OTFS radar [18]. The sequence $\mathbf{s}$ in (3) after CP addition is passed through a digital-to-analog convertor which derives the time domain transmit signal $s\,(t)$.

B. OTFS SAR CHANNEL MODEL

We consider a single set of fast time data for analysis i.e. sampled response of swath for a single transmit OTFS pulse. We assume that the velocity of the SAR platform is known to the operator with the aid of SAR geometry and on-board sensors. The response of the target swath for a single transmit pulse is a P-tap narrowband, doubly selective radar channel model which is represented as

$$h\,(\tau, \nu) = \sum\nolimits_{p=1}^{P} h_p \delta\left(\tau - \tau_p\right)\delta\left(\nu - \nu_p\right) \tag{4}$$

where $\delta(\cdot)$ is the dirac delta function, h_p is complex gain of the pth reflector, while τ_p and ν_p denote round-trip delay and Doppler shift of the pth reflector, respectively [18]. Round-trip delay and Doppler shift of the pth reflector are expressed as $\tau_p = l_p/M\Delta f$ and $\nu_p = k_p/NT$, where l_p and k_p are integers. The OTFS framework for SAR considers the delay and Doppler shift as integer multiples of the delay resolution $1/M\Delta f$ and Doppler resolution $1/NT$, respectively, the ranges for delay is $[0, T]$ and Doppler shift is $(-\frac{1}{2T}, \frac{1}{2T}]$, respectively. Since, the delay of received echo in SAR applications ranges from $(\tau_{min}, \tau_{max}]$ hence, the symbol duration $T \geq (\tau_{max} - \tau_{\text{min}})$ in CP-OTFS-based SAR.

The conventional SAR signal processing considers negligible Doppler shift within a single receive pulse at lower carrier frequencies [1], [2], [3] however, in mmWave band SAR operations this intra-pulse Doppler shift is discernible. We consider this intra-pulse Doppler to be induced by platform movement only, as the targets in the swath are assumed to be static. It is known that the swath size is typically much less than the distance between SAR and swath centre hence, at a particular slow-time a common look angle for the reflectors can be considered. Therefore, the common intra-pulse Doppler shift at a given slow-time can be given as $\nu_o = \frac{2V_p}{\lambda_c}$, where V_p is the platform velocity with respect to swath centre (known to the operator) and λ_c is the wavelength of carrier. This intra-pulse Doppler shift in CP-OTFS-based SAR will be ranging between $(-\frac{1}{2T}, \frac{1}{2T}]$ i.e. $|\nu_o| \leq \frac{1}{2T}$. The delay-Doppler domain SAR channel model at a given slow-time is given as

$$h\,(\tau, \nu) = \sum\nolimits_{l=0}^{M-1}\sum\nolimits_{k=0}^{N-1} h_{l,k}\delta\left(\tau - \frac{l}{M\Delta f}\right) \times \delta\left(\nu_o - \frac{(k)_N}{NT}\right) \tag{5}$$

where

$$(k)_N = \begin{cases} k & \text{if } k \leq N/2 \\ k - N & \text{otherwise} \end{cases}$$

and $h_{l,k}$ denotes the complex gain of swath at delay tap l and Doppler tap k corresponding to delay $l/M\Delta f$ and Doppler frequency $\frac{(k)_N}{NT}$, respectively, the tap $l = 0$ corresponds to the beginning of swath. As discussed, the reflectors have a common Doppler shift hence, (5) will have $h_{l,k} = 0$ for the indices $(k)_N \neq \nu_o NT$ (ν_o is integer multiple of $1/NT$). The SAR received signal $r\,(t)$ can be expressed as

$$r\,(t) = \iint h\,(\tau, \nu)\, s(t-\tau) e^{j2\pi\nu(t-\tau)} d\tau d\nu \tag{6}$$

C. CP-OTFS SAR DEMODULATOR

The OTFS receiver on reception of $r\,(t)$ removes CP from head and tail, and samples it at an interval T_s which is represented as vector $\mathbf{r} = \{r_n\}_{n=0}^{MN-1}$ with entries as

$$\mathbf{r} = \sum\nolimits_{p=1}^{P} h_p e^{j2\pi\frac{k_o(n-l_p)}{MN}} \mathrm{s}_{[n-l_p]_M} + \mathbf{w} \tag{7}$$

where $k_o = \nu_o NT$ represents the common Doppler tap and $\boldsymbol{w}$ is additive white Gaussian noise vector of length K with variance σ^2. The receiver devectorizes $\mathbf{r}$ into $M \times N$ matrix $\mathbf{R}$ and applies "Wigner transform". The transformation is performed as matched filtering operation with a pulse g_{rx} of duration $(0, T]$ followed by M-point Fast Fourier Transform (FFT). Lastly, a 2-dimensional (2D) Symplectic Fast Fourier Transform (SFFT) is applied and the demodulated two-dimensional delay-Doppler domain samples $\{y_{l,k}\}$, $l \in [0, M-1], k \in [0, N-1]$ are retrieved as $M \times N$ matrix $\mathbf{Y}$ as

$$\mathbf{Y} = \mathbf{F}_{\mathbf{M}}^{\mathbf{H}}\left(\mathbf{F}_{\mathbf{M}}\mathbf{G}_{\text{rx}}\mathbf{R}\right)\mathbf{F}_{\mathbf{N}} + \mathbf{W} \tag{8}$$

where G_{rx} is the diagonal matrix with entries as samples of g_{rx}: $G_{rx} = \text{diag}\left(g_{rx_0}, g_{rx_1}, \ldots, g_{rx_{(M-1)}}\right)$ and the M × N matrix W is additive white Gaussian noise with terms $w_{l,k} \sim \mathcal{CN}(0,\sigma^2)$. We choose, g_{rx} to be a rectangular pulse i.e. G_{rx} reduces to I_M. The statistical properties of w remains unchanged in (8) as all the operations are unitary. The exact relation between X and Y in delay-Doppler domain with rectangular pulses g_{tx} (t) and g_{rx} (t) is given as [23]

$$y_{l,k} = \sum_{l''=0}^{M-1}\sum_{k''=0}^{N-1} h_{l'',k''} e^{j2\pi\left(\frac{\left[l-l''\right]_M}{M}\right)\frac{\left(k''\right)_N}{N}} \alpha_{l,k} \times x_{\left[l-l''\right]_M,\left[k-k''\right]_N} + w_{l,k} \tag{9}$$

where

$$\alpha_{l,k} = \begin{cases} 1 & l'' \le l < M \\ e^{-j2\pi\frac{k}{N}} & 0 \le l < l'' \end{cases}$$

where the Doppler tap k'' will correspond to the Doppler frequency ν_o.

III. LOW COMPLEXITY RECEIVER FOR CP-OTFS SAR

In this section, we derive low complexity SAR receiver algorithm for intra-pulse Doppler compensation and IRCI-free range compression and analyze SNR.

A. DOPPLER COMPENSATION AND IRCI-FREE RANGE COMPRESSION

The receiver forms N vectors of dimension $M \times 1$ from the columns of $\mathbf{Y}$ and processes them independently based on the input-output relation obtained from (9). The relation between the input-output vectors is expressed as

$$\tilde{y}_{k'} = \boldsymbol{H}_{k'}\tilde{x}_{k'} + \tilde{w}_{k'} \tag{10}$$

where vectors $\tilde{y}_{k'}$ and $\tilde{w}_{k'}$ are the k'-th column of $\mathbf{Y}$ and $\mathbf{W}$, respectively, $k' \in [0, N-1]$. The vector $\tilde{x}_{k'} = [x_{0,[k'-k_o]_N} z^{0k_o}, x_{1,[k'-k_o]_N} z^{1k_o}, \ldots, x_{M-1,[k'-k_o]_N} z^{(M-1)k_o}]^T$, where $z = e^{j\frac{2\pi}{MN}}$ and the $M \times M$ channel matrix $\boldsymbol{H}_{k'}$ is

$$\boldsymbol{H}_{k'} = \begin{pmatrix} h_{0,(k_o)_N} & h_{M-1,(k_o)_N} W_N^{k'} & \cdots & h_{1,(k_o)_N} W_N^{k'} \\ h_{1,(k_o)_N} & h_{0,(k_o)_N} & \cdots & h_{2,(k_o)_N} W_N^{k'} \\ \vdots & \ddots & \ddots & \vdots \\ h_{M-1,(k_o)_N} & \cdots & h_{1,(k_o)_N} & h_{0,(k_o)_N} \end{pmatrix} \tag{11}$$

We observe that the entries above the main diagonal are multiplied by the same factor $W_N^{k'}$ thus, forming $\boldsymbol{H}_{k'}$ a factor circulant matrix. We now derive an efficient algorithm to estimate the complex gain of reflectors and eliminate the Doppler phase term $z^{(M-1)k_o}$. Since, the matrix $\boldsymbol{H}_{k'}$ is a factor-circulant matrix hence, it can be represented as [24, Theorem 1]

$$\boldsymbol{H}_{k'} = \boldsymbol{\mathcal{K}}_{k'}\mathbf{F}_\mathbf{M}^\mathbf{H}\mathbf{D}_{k'}\mathbf{F}_\mathbf{M}\boldsymbol{\mathcal{K}}_{k'}^{-1} \tag{12}$$

where $\boldsymbol{\mathcal{K}}_{k'} = diag\left(1, W_{MN}^{-k'}, W_{MN}^{-2k'}, \ldots, W_{MN}^{-(M-1)k'}\right)$ and $\boldsymbol{D}_{k'} = diag(\mathbf{F}_\mathbf{M}\boldsymbol{\mathcal{K}}_{k'}^{-1}(\sqrt{M}\mathbf{h}))$, while $\mathbf{h} = [h_{0,(k_o)_N}, \ldots\ldots\ldots, h_{M-2,(k_o)_N}, h_{M-1,(k_o)_N}]^T$. So, (10) can alternatively be represented as

$$\boldsymbol{y}_{k'} = \boldsymbol{\mathcal{K}}_{k'}\mathbf{F}_\mathbf{M}^\mathbf{H}\mathbf{D}_{k'}\mathbf{F}_\mathbf{M}\boldsymbol{\mathcal{K}}_{k'}^{-1}\tilde{x}_{k'} + \tilde{w}_{k'} \tag{13}$$

The received vector $\mathbf{y}_{k'}$ is pre-multiplied by $\boldsymbol{\mathcal{K}}_{k'}^{-1}$ followed by M-point FFT which is expressed as

$$\mathbf{F}_\mathbf{M}\boldsymbol{\mathcal{K}}_{k'}^{-1}\boldsymbol{y}_{k'} = \mathbf{D}_{k'}\mathbf{F}_\mathbf{M}\boldsymbol{\mathcal{K}}_{k'}^{-1}\tilde{x}_{k'} + \mathbf{F}_\mathbf{M}\boldsymbol{\mathcal{K}}_{k'}^{-1}\tilde{w}_{k'} \tag{14}$$

Notice that, $\mathbf{D}_{k'}$ is $M \times M$ diagonal matrix and $\mathbf{F}_\mathbf{M}\boldsymbol{\mathcal{K}}_{k'}^{-1}\tilde{x}_{k'}$ is $M \times 1$ column vector so we can express $\mathbf{D}_{k'}\mathbf{F}_\mathbf{M}\boldsymbol{\mathcal{K}}_{k'}^{-1}\tilde{x}_{k'} = \boldsymbol{D}'_{k'} \circ \mathbf{F}_\mathbf{M}\boldsymbol{\mathcal{K}}_{k'}^{-1}\tilde{x}_{k'}$, where $\boldsymbol{D}'_{k'} = \mathbf{F}_\mathbf{M}\boldsymbol{\mathcal{K}}_{k'}^{-1}(\sqrt{M}\mathbf{h}) \in \mathbb{C}^{M\times 1}$

Since, the SAR receiver has perfect knowledge of $\tilde{x}_{k'}$, element-wise division is carried out to estimate $\mathbf{D}'_{k'}$ as

$$\begin{aligned}\widehat{\boldsymbol{D}}'_{k'} &= \mathbf{F}_\mathbf{M}\boldsymbol{\mathcal{K}}_{k'}^{-1}\mathbf{y}_{k'} \oslash \mathbf{F}_\mathbf{M}\boldsymbol{\mathcal{K}}_{k'}^{-1}\tilde{x}_{k'} \\ &= \boldsymbol{D}'_{k'} + \mathbf{F}_\mathbf{M}\boldsymbol{\mathcal{K}}_{k'}^{-1}\tilde{w}_{k'} \oslash \mathbf{F}_\mathbf{M}\boldsymbol{\mathcal{K}}_{k'}^{-1}\tilde{x}_{k'}\end{aligned} \tag{15}$$

Finally, $\mathbf{h}$ is estimated by taking M-point IFFT of $\hat{D}'_{k'}$ followed by multiplication by $\boldsymbol{\mathcal{K}}_{k'}$ and we obtain

$$\begin{aligned}\hat{\mathbf{h}}_{k'} &= \boldsymbol{\mathcal{K}}_{k'}\mathbf{F}_\mathbf{M}^\mathbf{H}\mathbf{D}'_{k'} + \boldsymbol{\mathcal{K}}_{k'}\mathbf{F}_\mathbf{M}^\mathbf{H}(\mathbf{F}_\mathbf{M}\boldsymbol{\mathcal{K}}_{k'}^{-1}\tilde{w}_{k'} \oslash \mathbf{F}_\mathbf{M}\boldsymbol{\mathcal{K}}_{k'}^{-1}\tilde{x}_{k'}) \\ &= \sqrt{M}\mathbf{h} + \tilde{w}'_{k'}\end{aligned} \tag{16}$$

where $\tilde{w}'_{k'}$ is noise with variance as in (15). The estimate $\hat{h}_{k'}$ in (16) is a scaled version of $\mathbf{h}$ by a factor of $\sqrt{M}$ with an term of additive noise $\tilde{w}'_{k'}$. Therefore, we observe that the complex gains $\mathbf{h} = [h_{0,(k_o)_N}, h_{1,(k_o)_N}, h_{2,(k_o)_N} \ldots\ldots, h_{M-2,(k_o)_N}, h_{M-1,(k_o)_N}]^T$ of M reflectors are estimated without any addition by the coefficients of adjacent cells. Thus, $\mathbf{h}$ is perfectly recovered with a gain of $\sqrt{M}$ and is devoid of any IRCI from the adjacent cells. Notice that, $\mathbf{h}$ is perfectly recovered without any additional phase term due to intra-pulse Doppler shift. This compensation is due to the signal processing of the received OTFS signal in delay-Doppler domain.

The signal processing from (10) to (16) is only for M received samples, thus, in order to perform the range compression for all K samples, a complex addition is carried out for all N sub-matrices with the evaluated estimates. Note that, $\mathbf{h}$ is perfectly evaluated N times so, the complex addition is equivalent to a coherent integration which improves the SNR by a factor of N. The overall functionality of the proposed low-complexity receiver is given in Algorithm 1.

We note that the CP is dropped from head and tail of the receive signal and the receiver processes the signal only for a duration NT. Hence, the initial inactive time for the receiver will be for the duration NT. Therefore, the minimum range of CP-OTFS is similar to that of a pulsed radar i.e. $cNT/2$ where c is the speed of light.

Algorithm 1 Low Complexity CP-OTFS Receiver

1: Precomputed : $\mathcal{K}_{\mathbf{k}'_{M\times M'}}\mathcal{K}^{-1}_{\mathbf{k}'_{M\times M'}}(\mathbf{F_M}\mathcal{K}^{-1}_{\mathbf{k}'}\tilde{x}_{\mathbf{k}'})_{M\times 1}$
2: Given : a vector $\mathbf{R}_{M\times N}$
3: Output : $\mathbf{h}_{M\times 1}$
4: Compute : $\mathbf{Y}_{M\times N} = \mathbf{R}_{M\times N}\mathbf{F_N}$
5: **for** $k' = 0 : N-1$ **do**
6: **for** $l' = 0 : M-1$ **do**
7: Compute : $\mathbf{y}_{\mathbf{k}'_{M\times 1}} = \mathbf{Y}(k',l')_{M\times N}$
8: **end for**
9: Compute : $\mathbf{F_M}\mathcal{K}^{-1}_{\mathbf{k}'_{M\times M}}\mathbf{y}_{\mathbf{k}'_{M\times 1}}$
10: Compute: $\widehat{D}_{\mathbf{k}'}\times 1' = \left(\mathbf{F}_M\mathcal{K}_{\mathbf{k}'-\mathbf{1}}\mathbf{y}_{\mathbf{k}'}\right)_{M\times 1} \oslash \left(\mathbf{F_M}\mathcal{K}^{-1}_{k'}\tilde{\mathbf{x}}_{\mathbf{k}'}\right)_{M\times 1}$
11: Compute : $\hat{\mathbf{h}}_{k'_{M\times 1}} = \mathcal{K}_{k'_{M\times M}}\mathbf{F}^{\mathbf{H}}_{\mathbf{M}}\widehat{D}'_{k'M\times 1}$
12: **end for**
13: Compute : $\mathbf{h}_{M\times 1} = \sum_{k'=0^{N-1}}\hat{\mathbf{h}}_{\mathbf{k}'_{M\times 1}}$

B. SIGNAL-TO-NOISE RATIO ANALYSIS AFTER RANGE COMPRESSION

We now analyze the variation in noise power at each stage of the pulse compression. Since, FFT and multiplication of $\mathcal{K}^{-1}_{k'}$ in (14) are unitary operations hence, the noise variance of $\mathbf{F_M}\mathcal{K}^{-1}_{k'}\tilde{w}_{k'}$ remains same as that of $\tilde{w}_{k'}$ i.e.σ^2. We now define $\tilde{X}_{\mathbf{k}'} = \mathbf{F_M}\mathcal{K}^{-1}_{k'}\tilde{x}_{\mathbf{k}'} \in \mathbf{C}^{M\times 1}$ where, $\tilde{x}_{k'm}$ is the mth element of $\tilde{X}_{k'}$. In (15) the element-wise division with $\tilde{X}_{\mathbf{k}'}$ changes the noise variance of m-th element of $\tilde{w}_{\mathbf{k}'}$ to $\sigma^2 \Big/ (\tilde{x}_{k'm})^2$.

The receiver then carries out range compression by the IFFT operation and multiplication of $\mathcal{K}_{\mathbf{k}'}$ with the samples obtained in (15). Since, the IFFT and multiplication of $\mathcal{K}_{\mathbf{k}'}$ in (16) are unitary operations hence, the noise variance does not change from (15). The noise power in (16) for the $l-$th range cell after pulse compression is $\frac{\sigma^2}{M}\sum_{m=0}^{M-1}|\tilde{x}_{k'm}|^{-2}$. Thus, the SNR of $l-$th range cell after range compression in (16) is expressed as

$$\mathrm{SNR}_l = \frac{M\left|h_{l,(k)_N}\right|^2}{\frac{\sigma^2}{M}\sum_{m=0}^{M-1}|\tilde{x}_{k'm}|^{-2}} \tag{17}$$

We note that a larger SNR_l will be achieved with smaller value of $\sum_{m=0}^{M-1}|\tilde{x}_{k'm}|^{-2}$ if an optimal $\tilde{x}_{k'm}$ is chosen. We assume $\|\mathbf{S}\|^2 = 1$, i.e. transmit signal with normalized energy constraint so, for $\tilde{X}_{\mathbf{k}'}$ we have $\sum_{m=0}^{M-1}\tilde{x}^2_{k'm} = \frac{1}{N}$. When $\tilde{X}_{\mathbf{k}'}$ has constant modulus then, $|\tilde{x}_{k'0}| = |\tilde{x}_{k'1}| = \cdots = \left|\tilde{x}_{k'M-1}\right| = \frac{1}{\sqrt{MN}}$, and we achieve minimal value of $\sum_{m=0}^{M-1}\tilde{x}^{-2}_{k'm} = M^2N$. In this case, we achieve the maximal SNR_l after range compression as

$$\mathrm{SNR}_{max,l} = \frac{\left|h(l,(k)_N)\right|^2}{N\sigma^2} \tag{18}$$

After performing range compression for N vectors, the estimates of $\mathbf{h}$ is coherently integrated. The integration improves SNR by N and the overall maximal SNR becomes

$$\mathrm{SNR}_{max} = \frac{\left|h_{l,(k)_N}\right|^2}{\sigma^2} \tag{19}$$

Since, the mean power of $\mathbf{S}$ is $\frac{1}{\sqrt{MN}}$ the SNR of l-th range cell for the received signal before range compression is

$$\overline{\mathrm{SNR}}_l = \frac{\left|h_{l,(k)_N}\right|^2}{MN\sigma^2} \tag{20}$$

On comparing (19) and (20) we observe that the SNR has improved by a factor of MN after the range compression. This improvement is equal to the time-bandwidth product as in the case of LFM, OFDM and matched-filter OTFS radars, respectively [1], [13], [18]. We observe that the actual transmit duration of OTFS pulse is $(MN+L-1)T_s$ however, we discard the CP before pulse compression which results in minor difference of gain by $L-1$ since, $L-1 \ll MN$.

IV. RESULTS

In this section, we present the computational complexity of proposed pulse compression algorithm and give some simulation results.

A. COMPUTATIONAL COMPLEXITY

The computational complexity is calculated in terms of the required number of complex multiplications (CMs). The p-point FFT and IFFT require $\frac{p}{2}log_2(p)$ CMs. The CMs required for various operations in our proposed receiver is given in Table.1. It is evident that the overall computational complexity of CP-OTFS-based SAR is $O(MNlog_2(MN))$ which is superior to $O(M^3N^3)$ of direct matrix inversion OTFS receiver. The proposed receiver has higher computational efficiency in comparison to state-of-the-art matched-filter OTFS radar [18] which has a complexity of $O(M^2N^2)$. The comparison for receiver complexity in Fig.1. is plotted for $K \in [2, 8192]$. It can be observed that our proposed receiver algorithm requires almost 10^3 and 10^6 times lower CMs than the matched-filter OTFS and direct matrix inversion OTFS receiver, respectively. Thus, the result validates

TABLE 1. Computational complexity of various operations.

Operation	Number of Complex Multiplications
(8)	$\frac{MN}{2}log_2(N)$
(14)	$M+\frac{M}{2}log_2(M)$
$(\mathbf{F_M}\mathcal{K}^{-1}_{k'}\tilde{x}_{k'})_{M\times 1}$	$M+\frac{M}{2}log_2(M)$
(15,16)	$2M+\frac{M}{2}log_2(M)$
N loops of $(14-16)$	$4M+\frac{3M}{2}log_2(M)$
Total CMs $=$	$\frac{MN}{2}log_2(N)+4MN+\frac{3MN}{2}log_2(M)$ $=\frac{MN}{2}log_2(MN)+4MN+MNlog_2(M)$

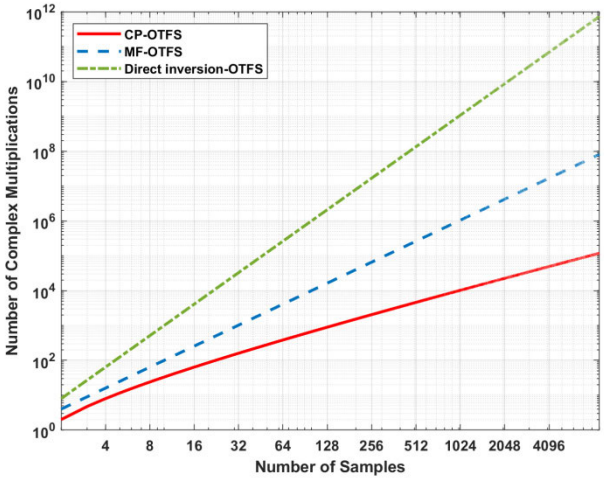

FIGURE 1. Computation complexity comparison of different receivers.

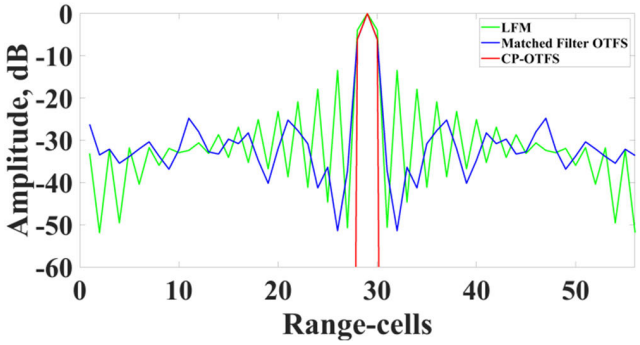

FIGURE 2. Normalized range profiles of the point spread function.

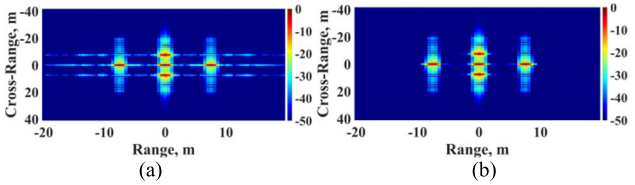

FIGURE 3. Simulated SAR images (a) Matched-filter OTFS SAR (b) CP-OTFS SAR.

suitability of our proposed algorithm over the other existing methodologies.

B. SIMULATIONS AND DISCUSSIONS

We simulate Spot-light SAR with Range Migration Algorithm having following simulation parameters: Carrier frequency f_c = 9GHz, Bandwidth B = 100MHz, transmit pulse-width (without CP) T = 30.72μs, receiver dynamic range = 50dB, synthetic aperture length = 60m, swath size = 40m × 40m, swath center = 5km and choose M = 192and$N$ = 16 for OTFS pulse. We do not consider white noise in simulations for ease of analysis.

The normalized range profile of point spread functions are shown in Fig. 2. The results clearly indicate that IRCI-free

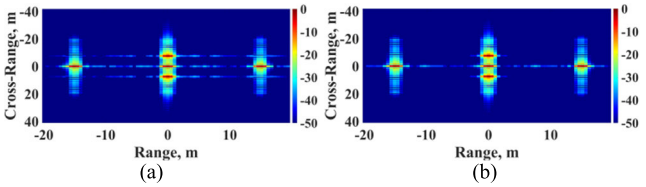

FIGURE 4. Simulated SAR images of OTFS-SAR with (a) 50% CP (b) 70% CP.

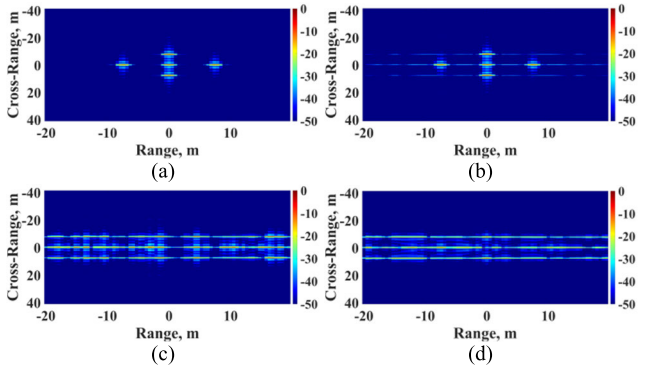

FIGURE 5. SAR images with intra-pulse Doppler shift: (a) CP-OTFS SAR (b) Matched-filter OTFS SAR (c) OFDM SAR (d) FDSI SAR.

range profiling is achieved by CP-OTFS while, the LFM and matched-filter OTFS radars show presence of high range side-lobes which interfere with the adjacent cells and cause IRCI. We observe that, the matched-filter OTFS radar has lower side-lobes as compared to LFM-based radar. However, the technique is still unsuitable for high resolution imaging applications as the SAR receivers have a typical dynamic range of 50dB and side-lobes of the order of −30dB will result in IRCI.

In Fig. 3. a superior performance of CP-OTFS-based imaging is observed over matched-filter OTFS SAR. The CP-OTFS-based SAR has zero IRCI from the adjoining cells whereas, the matched-filter OTFS-based technique results in presence of side-lobes which leads to inferior performance. We highlight that this enhanced performance is achieved at a much less computational cost thus, proving the efficiency of CP-OTFS-based technique. Fig. 4. highlights the significance of adding sufficient CP for achieving IRCI-free imaging. We observe that, CP corresponding to the number of range cells in swath has to be pre-fixed to the transmit pulse in order to achieve IRCI-free range profiling.

The distortion caused by intra-pulse Doppler shift at carrier frequency f_c = 77GHz and platform velocity of 228km/hr is shown in Fig.5. The CP-OTFS-based SAR effectively nullifies the distortion caused by intra-pulse Doppler vis-a-vis OFDM and FDSI based techniques [13], [14]. The matched-filter OTFS also counters the effect of intra-pulse Doppler shift however, presence of IRCI and high computational complexity makes it less suitable as compared to CP-OTFS-based SAR.

V. CONCLUSION

In this paper, a low complexity receiver algorithm for CP-OTFS-based SAR is proposed which effectively mitigates intra-pulse Doppler shift impairments and achieves IRCI-free imaging. This low complexity pulse compression algorithm was derived by exploiting the diagonalization property of the factor-circulant matrix. The novel delay-Doppler domain based signal processing was shown to be effective in nullifying the effects of intra-pulse Doppler shift in mmWave band SAR imaging. The proposed technique achieved high resolution IRCI-free imaging while the pulse compression gain was shown to be equal to the time-bandwidth product. The computational complexity of the receiver algorithm was shown to be $O(MNlog_2(MN))$ which is superior to $O(M^2N^2)$ of the matched-filter OTFS radar. Simulation results exhibited high quality IRCI-free imaging capabilities of our proposed algorithm vis-a-vis state-of-the-art matched-filter OTFS radar. In future studies, the authors intend to investigate OTFS for fractional intra-pulse Doppler shifts in SAR imaging.

REFERENCES

[1] I. G. Cumming and F. H. Wong, *Digital Processing of Synthetic Aperture Radar Data: Algorithms and Implementation*. Norwood, MA, USA: Artech House, 2005.

[2] M. Soumekh, *Synthetic Aperture Radar Signal Processing*. New York, NY, USA: Wiley, 1999.

[3] J. C. Curlander and R. N. McDonough, *Synthetic Aperture Radar: Systems and Signal Processing*. Hoboken, NJ, USA: Wiley, 1991.

[4] M. E. Yanik, D. Wang, and M. Torlak, "Development and demonstration of MIMO-SAR mmWave imaging testbeds," *IEEE Access*, vol. 8, pp. 126019–126038, 2020, doi: 10.1109/ACCESS.2020.3007877.

[5] M. Schmitt and X. X. Zhu, "Demonstration of single-pass millimeterwave SAR tomography for forest volumes," *IEEE Geosci. Remote Sens. Lett.*, vol. 13, no. 2, pp. 202–206, Feb. 2016, doi: 10.1109/LGRS.2015.2506150.

[6] X. Gao, S. Roy, and G. Xing, "MIMO-SAR: A hierarchical high-resolution imaging algorithm for mmWave FMCW radar in autonomous driving," *IEEE Trans. Veh. Technol.*, vol. 70, no. 8, pp. 7322–7334, Aug. 2021, doi: 10.1109/TVT.2021.3092355.

[7] G. Wu, K. F. Chan, K. M. Shum, and C. H. Chan, "Millimeter-wave and terahertz OAM discrete-lens antennas for 5G and beyond," *IEEE Commun. Mag.*, vol. 60, no. 1, pp. 34–39, Jan. 2022, doi: 10.1109/MCOM.001.2100523.

[8] E. Björnson, J. Hoydis, and L. Sanguinetti, "Massive MIMO has unlimited capacity," *IEEE Trans. Wireless Commun.*, vol. 17, no. 1, pp. 574–590, Jan. 2018, doi: 10.1109/TWC.2017.2768423.

[9] S. Fortunati, L. Sanguinetti, F. Gini, M. S. Greco, and B. Himed, "Massive MIMO radar for target detection," *IEEE Trans. Signal Process.*, vol. 68, pp. 859–871, 2020, doi: 10.1109/TSP.2020.2967181.

[10] F. Guidi, A. Guerra, and D. Dardari, "Personal mobile radars with millimeter-wave massive arrays for indoor mapping," *IEEE Trans. Mobile Comput.*, vol. 15, no. 6, pp. 1471–1484, Jun. 2016, doi: 10.1109/TMC.2015.2467373.

[11] A. Sakhnini, S. De Bast, M. Guenach, A. Bourdoux, H. Sahli, and S. Pollin, "Near-field coherent radar sensing using a massive MIMO communication testbed," *IEEE Trans. Wireless Commun.*, vol. 21, no. 8, pp. 6256–6270, Aug. 2022, doi: 10.1109/TWC.2022.3148035.

[12] M. A. Richards, *Fundamentals of Radar Signal Processing*. New York, NY, USA: McGraw-Hill, 2014.

[13] T. Zhang and X. Xia, "OFDM synthetic aperture radar imaging with sufficient cyclic prefix," *IEEE Trans. Geosci. Remote Sens.*, vol. 53, no. 1, pp. 394–404, Jan. 2015, doi: 10.1109/TGRS.2014.2322813.

[14] C. Tierney and B. Mulgrew, "Waveform independent range profile reconstruction for SAR," in *Proc. Int. Conf. Radar Syst. (Radar)*, Oct. 2017, pp. 1–6, doi: 10.1049/cp.2017.0460.

[15] Y. Cao and X. Xia, "IRCI-free MIMO-OFDM SAR using circularly shifted Zadoff–Chu sequences," *IEEE Geosci. Remote Sens. Lett.*, vol. 12, no. 5, pp. 1126–1130, May 2015, doi: 10.1109/LGRS.2014.2385693.

[16] M. Alshaya, M. Yaghoobi, and B. Mulgrew, "High-resolution wide-swath IRCI-free MIMO SAR," *IEEE Trans. Geosci. Remote Sens.*, vol. 58, no. 1, pp. 713–725, Jan. 2020, doi: 10.1109/TGRS.2019.2940075.

[17] R. Hadani, S. Rakib, M. Tsatsanis, A. Monk, A. J. Goldsmith, A. F. Molisch, and R. Calderbank, "Orthogonal time frequency space modulation," in *Proc. IEEE Wireless Commun. Netw. Conf. (WCNC)*, San Francisco, CA, USA, Mar. 2017, pp. 1–6, doi: 10.1109/WCNC.2017.7925924.

[18] P. Raviteja, K. T. Phan, Y. Hong, and E. Viterbo, "Orthogonal time frequency space (OTFS) modulation based radar system," in *Proc. IEEE Radar Conf. (RadarConf)*, Boston, MA, USA, Apr. 2019, pp. 1–6, doi: 10.1109/RADAR.2019.8835764.

[19] S. Tiwari, S. S. Das, and V. Rangamgari, "Low complexity LMMSE receiver for OTFS," *IEEE Commun. Lett.*, vol. 23, no. 12, pp. 2205–2209, Dec. 2019, doi: 10.1109/LCOMM.2019.2945564.

[20] M. A. Sheikh, P. Singh, and R. Budhiraja, "Low-complexity MMSE receiver design for massive MIMO OTFS systems," *IEEE Commun. Lett.*, vol. 26, no. 11, pp. 2759–2763, Nov. 2022, doi: 10.1109/LCOMM.2022.3198136.

[21] Z. Gong, S. Liu, and Y. Huang, "Doppler diversity reception for OTFS modulation," in *Proc. IEEE 95th Veh. Technol. Conference: (VTC-Spring)*, Helsinki, Finland, Jun. 2022, pp. 1–5, doi: 10.1109/VTC2022-Spring54318.2022.9860675.

[22] H. Bi, G. Bi, B. Zhang, W. Hong, and Y. Wu, "From theory to application: Real-time sparse SAR imaging," *IEEE Trans. Geosci. Remote Sens.*, vol. 58, no. 4, pp. 2928–2936, Apr. 2020, doi: 10.1109/TGRS.2019.2958067.

[23] P. Raviteja, Y. Hong, E. Viterbo, and E. Biglieri, "Practical pulse-shaping waveforms for reduced-cyclic-prefix OTFS," *IEEE Trans. Veh. Technol.*, vol. 68, no. 1, pp. 957–961, Jan. 2019, doi: 10.1109/TVT.2018.2878891.

[24] J. C. R. Claeyssen and L. A. D. S. Leal, "Diagonalization and spectral decomposition of factor block circulant matrices," *Linear Algebra Appl.*, vol. 99, pp. 41–61, Feb. 1988.

GAURAV SHARMA (Graduate Student Member, IEEE) received the B.Tech. degree in electronics and communication engineering from Chhatrapati Shahu Ji Maharaj University, Kanpur, India, in 2001, and the M.Tech. degree in telecom systems engineering from the Indian Institute of Technology, Kharagpur, India, in 2011. He is currently pursuing the Ph.D. degree in the field of radar signal processing with the Defence Institute of Advanced Technology, Pune, India. His current research interests include signal processing of modern waveforms for synthetic aperture radar (SAR) image processing and integrated sensing and communication.

A. AROCKIA BAZIL RAJ (Senior Member, IEEE) received the B.E. degree in electronics and communication engineering from Bharathidasan University, Tiruchirappalli, India, and the M.E. degree in communication systems and the Ph.D. degree in information and communication technology from Anna University, Chennai, India.

He was an Assistant Professor with the Kings College of Engineering, Thanjavur, India, from 2002 to 2006, where he was promoted to Associate Professor with the Research, Development and Establishment Section, from 2007 to 2015. He has been an Associate Professor with the Defence Institute of Advanced Technology, Pune, India, since 2015. His Ph.D. research was supported by the Defence Research and Development Organization, New Delhi, India, under the Extramural Research (ER) and Intellectual Property Rights (IPR) Project Grant. He has authored a number of research articles and three books. His current research interests include free-space optics (FSO) communications, digital signal processing, RF photonics, and radar signal processing.